Journal of Catalysis **186,** 296–309 (1999)
Article ID jcat.1999.2577, available online at http://www.idealibrary.com on IDEAL®

Chemisorption and Reaction of NO and N_2O on Oxidized and Reduced Ceria Surfaces Studied by Soft X-Ray Photoemission Spectroscopy and Desorption Spectroscopy

S. H. Overbury,[1] D. R. Mullins, D. R. Huntley,[2] and Lj. Kundakovic

Oak Ridge National Laboratory, P.O. Box 2008, Building 4500 N, MS 6201, Oak Ridge, Tennessee 37831-6201

Received January 4, 1999; revised May 28, 1999; accepted May 28, 1999

We have examined the chemisorption and reaction of NO and N_2O on ceria surfaces by soft X-ray photoelectron spectroscopy (SXPS), X-ray absorption spectroscopy, and isothermal and temperature programmed desorption (TPD) spectroscopy. Samples include highly oriented CeO_2(100) and CeO_2(111) thin films with surfaces of variable oxidation states. CeO_2(111) thin films were grown *in situ* **allowing control over the initial oxidation state of the ceria surface, quantitatively determined by valence band, Ce 4*d*, and Ce 3*d* photoemission. Following NO exposure, various N-containing surface species were observed by N 1*s* photoemission, and the distribution of these species depended upon surface oxidation state, exposure, and adsorption temperature. These species included N_2O, nitrite, NO^-, and three states believed to be associated with atomic or anionic forms of N. Nitrite and N_2O are seen on a fully oxidized surface while NO^-, N_2O, and dissociation products are observed on a reduced surface. The primary reaction of NO with reduced ceria is reoxidation of the ceria by the NO, both by NO^- formation and by NO dissociation, leading to immediate and thermally induced N_2 desorption. Adsorption of NO at 150 K is predominantly molecular while exposure to NO at 400 K leads to a thermally activated nitride which desorbs at temperatures above 500 K. Dissociative adsorption of NO leads to the displacement of N^{3-} at high exposures.**

Key Words: **NO reduction; NO, nitric oxide; N_2O, nitrous oxide; ceria, CeO_2; X-ray photoelectron spectroscopy; near edge x-ray absorption spectroscopy; thermal desorption spectroscopy.**

1. INTRODUCTION

There is considerable evidence that reducible metal oxide supports play a complex role in oxidation and reduction catalysis. In automotive catalytic converters, ceria additions are known to have the effect of diminishing activity fluctuations caused by changes in exhaust gas air to fuel ratio (1, 2). In this role, ceria is known to participate in both CO oxidation and NO reduction through oxygen storage and synergistic interactions with the supported metal (3–9). Metal oxides are known to have catalytic activity for both direct decomposition and selective catalytic reduction of NO (10, 11). Zhang and Vannice have compared several doped and undoped rare earth and transition metal oxides and find reversible and irreversible NO uptake by these catalysts and wide variation in their activities for NO reduction (11). It is not clear what factors control this variability nor what active and spectator species are present on the catalyst surface under conditions of direct and selective reduction of NO.

Various techniques have been applied to characterize the interaction between reducible oxide surfaces and NO. Fourier transform infrared (FTIR) studies have revealed that many types of species result from NO exposure and have revealed pronounced variation between different oxide surfaces. Oxides studied by FTIR include titania (12–15), chromia (16, 17), tin oxide (18), manganese oxide (19), ceria (20–22), and mixed oxides such as ceria/titania (23). In many cases, the state of the oxide substrate may not be well known, since the oxidation state of the oxide is not directly obtained from FTIR. The nature of the adsorbed species depends upon careful sample pretreatments, and previous studies were often performed without other direct probes of how these factors affect the oxides. Electron spin resonance (ESR) detects NO radicals but is blind to other nitrogen containing species. A recent review by Trovarelli discusses the conclusions from previously published studies of NO on high surface area ceria (24). Surface studies of model single crystal surfaces could help clarify the structural and reactivity aspects of this interaction. A tabulation of NO adsorption studies indicates that there have really been very few such studies of NO chemisorption on single crystal oxide surfaces (25).

[1] To whom correspondence should be addressed. E-mail: overburysh@ornl.gov. Fax: (423)576-5235.

[2] Current address: Saginaw Valley State University, Department of Chemistry, University Center, MI 48710-0001.

0021-9517/99 $30.00

In this paper, we report on experiments which use soft X-ray photoemission, X-ray absorption, and thermal desorption spectroscopy to study the interaction of NO with highly oriented, crystalline ceria surfaces. Using valence band and Ce 4*d* photoemission, the extent of reduction of the ceria surfaces could be quantitatively determined. Using ceria films produced by various methods we have been able to prepare surfaces with an arbitrary extent of reduction. Following NO exposure on these surfaces, we have used photoemission and X-ray absorption as probes of the chemical state of the N and O species. We find at least six distinguishable N containing species and have determined their evolution with temperature and their dependence upon adsorption temperature, coverage, extent of the ceria reduction and observed desorption products.

2. EXPERIMENTAL METHODS

These experiments were performed in two different UHV chambers. The soft X-ray photoemission and photoabsorption experiments were conducted at the National Synchrotron Light Source at beamline X-1B using photon energies ranging from 290 to 600 eV, but nominally 545 eV for the N 1*s* photoemission spectra. The end-station chamber contained a VSW EA125 electrostatic analyzer operated in the constant pass energy mode for photoemission measurements. A partial yield detector was used for X-ray absorption measurements. Photon energies were calibrated by comparison of photoelectron kinetic energies excited by first- and second-order X-rays emitted from the monochromator. Sample dosing of NO and N_2O was performed using a directed doser, configured to enhance exposure of the front surface compared to the back and sides of the sample. The dosing rate was controlled by a laser drilled effusion aperture and adjusted by the pressure in a gas ballast behind the aperture. Exposures are approximately calibrated by comparing with gas uptake measurements performed by backfilling the chamber. Exposures are therefore given in Langmuirs ($1\ \mathrm{L} = 10^{-6}$ Torr s). A second UHV system was used for the isothermal and temperature programmed desorption measurements. It was equipped with XPS capabilities to permit characterization of the oxidation state of the surface utilizing the Ce 3*d* core levels. Gas dosing was performed using a nearly identical gas doser as in the first UHV system. In this apparatus, isotopically labeled ^{15}NO was used to reduce interference from ambient gas during TPD and isothermal desorption measurements.

Ceria surfaces with two principle crystallographic orientations, the (100) and (111), were used. Two methods were used to produce (111) films. In one method, ultrathin films of ceria (<5 nm thick) were grown in UHV using Ru(0001) as a substrate. An evaporative cerium metal source was operated in the SXPS system. The oxygen pressure and Ce dose rate were adjusted so that the oxygen would be more than sufficient to fully oxidize the Ce as it was deposited. The films were grown at a substrate temperature of 700 K which was found to yield optimal crystallinity. It is found by ion scattering and LEED results (26) that CeO_2 grown on this substrate produces films oriented with $CeO_2(111)//Ru(0001)$ and $CeO_2[110]//Ru\ [11\bar{2}0]$. A second type of sample was in the form of thicker films (50 nm) grown *ex situ* on biaxially rolled Ni substrates (27). These films were found by X-ray diffraction (XRD) to be oriented primarily to (111) with a rocking curve width of about 8°.

Two types of (100) samples were used. One type of $CeO_2(100)$ was grown by laser ablation onto polished single crystal $SrTiO_3(100)$ substrates (STO) as described previously (8, 28). These films were typically 500 nm thick and exhibited XRD rocking curve and ϕ scans with full widths of 1.4° and 0.7°, respectively, indicating epitaxial growth with $CeO_2(100)//SrTiO_3(100)$ and $CeO_2[010]//SrTiO_3[010]$. Another was prepared by vapor deposition of ceria onto biaxially rolled Ni produced as described elsewhere (27). These films were also oriented to (100) but had a lower degree of azimuthal alignment of CeO_2 crystallites as indicated by X-ray rocking curves (27). Finally, in one set of experiments a polycrystalline Ce foil was mounted in UHV and treated with oxygen to produce either a fully oxidized or a partially oxidized overlayer, as described earlier (29).

Control over the extent of reduction of these surfaces was obtained in different ways. For the thicker films grown on Ni and STO, highly reduced surfaces could be obtained by sputtering the surface, leading to the preferential removal of O. However, the oxidation state of these surfaces was unstable due to outward diffusion of oxygen from the subsurface region. For the ultrathin films grown on Ru(0001), oxidation state was controlled by the variation of the oxygen pressure during deposition. Following deposition of a fully oxidized film, a thin overlayer of reduced CeO_x was deposited on top by deposition at a reduced oxygen pressure. Due to the limited amount of subsurface oxygen available, the oxidation state of these surfaces were very stable to annealing at high temperatures. Although accurate estimates of the film thicknesses were not available, they were typically sufficient to completely attenuate the Ru signal in AES and SXPS, but thin enough that they could be readily and completely removed by ion sputtering for 10 to 20 min.

The extent of reduction of the resulting ceria film can be measured from the Ce 4*d*, Ce 3*d*, or the valence band (VB) spectrum (29, 30). A parameterization describing the oxidation state of the surface was developed based on all data from surfaces prepared over the full range of oxidation from Ce^{3+} to Ce^{4+}. Surfaces which were exposed to oxygen at 500 K followed by high temperature anneals yielded highly oxidized surfaces which were taken to be 100% Ce^{4+}. These were characterized by zero intensity of the Ce 4*f* peak in the valence band spectrum and zero intensity of the D peak in the Ce 4*d* spectrum (29). Highly reduced surfaces, having

essentially all Ce visible to the photoemission probes existing in the Ce^{3+} state (0% Ce^{4+}), exhibited complete loss of the X''' and U''' peaks in the Ce 4*d* and 3*d* spectra, respectively (29). Using the relative intensities of these peaks it is possible to estimate the relative amounts of Ce^{4+} and Ce^{3+} for any surface to within about 10%. The fraction of oxidized Ce, expressed as $f^{4+} = Ce^{4+}/(Ce^{3+} + Ce^{4+})$, is used to describe the extent of oxidation of the surface. However, this oxidation state is an average value over the depth weighted distribution probed by the photoelectrons. The kinetic energies of the Ce 4*d*, Ce 3*d*, and Ce 4*f* electrons used in this analysis were approximately 400, 360, and 290 eV, resulting from nominal photon excitation energies of 525, 1253, and 295 eV, respectively.

Certain of the N containing species were sensitive to X-ray exposure. Their sensitivity was checked by measurements of peak intensities vs X-ray exposure time. Various procedures (variation of X-ray incidence point on sample, flux stops, and minimal counting times) were used to minimize or account for these affects.

3. RESULTS

3.1. Surface Species Formed during Isothermal Adsorption

NO uptake readily occurs on a reduced CeO_2 surface, but the species obtained depend upon the temperature at which the NO was adsorbed. This is demonstrated by the spectra in Fig. 1 which show adsorption at different temperatures

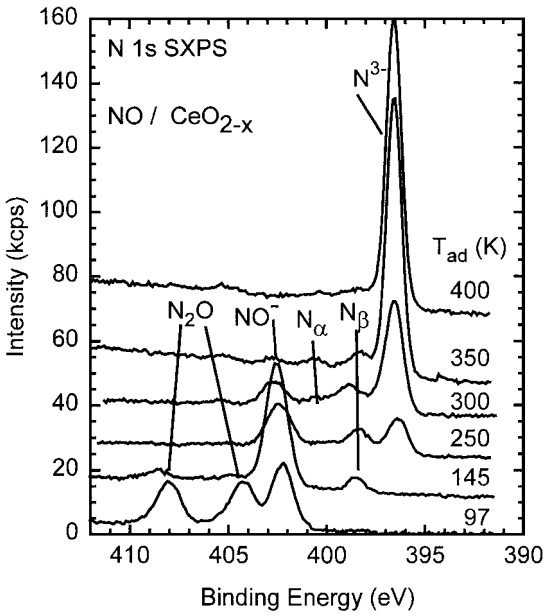

FIG. 1. N 1*s* SXPS spectra resulting from 20 L exposure to NO at various different surface temperatures. The substrate was a reduced CeO_2 film grown upon Ru(0001). The initial oxidation state of the CeO_2 substrate varied from 3 to 26% oxidized prior to NO exposure and varied from 44 to 76% oxidized immediately following exposure, as determined from the Ce 4*d* spectra.

TABLE 1

Peak Positions of Features Seen in N 1*s* for Oxidized or Reduced CeO_2[a]

Assignment	Shift from nitride (eV)	Binding energy (eV)[b]
N^{3-} nitride	0	396.5
N_β-anionic N at defects	2.1	398.6
N_α-anionic N at defects	4.0	400.5
NO^-	6.1	402.6
N_2O peak 1[c]	8.1	404.6
nitrite[d]	9.2	405.7
N_2O-peak 2[c]	11.8	408.3

[a] For CeO_2(111) surface grown of Ru(0001).
[b] Referenced to the X''' peak in the Ce 4*d* spectra (29).
[c] Measured with respect to NO^- in absence of nitride.
[d] Measured with respect to N_2O peaks in absence of nitride by curve fitting to resolve features.

on a reduced ceria film grown on CeO_2(111)/Ru(0001). The spectra in Fig. 1 were obtained at low temperatures following exposing the sample to 20 L of NO at the indicated temperatures. The binding energy scale was obtained by referencing to the X''' peak in the Ce 4*d* spectrum (binding energy 122.8 eV (29)) measured just before or after the NO adsorption, using the techniques described in an earlier publication (29). The binding energies of various features are summarized in Table 1.

Exposure near 100 K on a reduced surface yields three prominent peaks in the N 1*s* spectrum. The two peaks at highest binding energy are assigned to N contained in N_2O. On reduced surfaces, these two peaks always appeared together and with unity intensity ratio. The energy difference between these two peaks was 3.8 eV and the binding energies, 408.3 and 404.6 eV, were consistent with those measured from N_2O adsorbed on passivated metal surfaces reported in the literature and given in Table 2. This assignment was further confirmed by performing direct

TABLE 2

Binding Energies for Adsorption of N_2O or NO on Various Samples

Adsorbate/Substrate	N*NO	NN*O	Splitting	Ratio	NO
$N_2O/Rh/CeO_2$	403.8	407.6	3.8	0.99	—
N_2O/CeO_x	NA	NA	3.8	1.01	—
NO/CeO_x	404.6	408.3	3.8	0.98	402.6[a]
$NO/Rh/CeO_x$	404.1	407.9	3.8	1.04	402.1[a]
NO/Ru(0001) present					400.0
α-N_2O, ($v1 + v2$)NO/Ru(0001) (32, 31, 46)	401.6	405.6	4.0		400.0
N_2O, NO/$p(2 \times 2)$–O–W(100) (43)	402.7	406.4	3.7		404
N_2O, NO/oxidized Al(100) (44)	403.5	407.4	3.9		403.1

[a] Binding energy of NO^- state.

adsorption of gaseous N_2O on reduced CeO_2 and upon a highly oxidized CeO_2 surface which had Rh deposited upon it. These yielded identical values of the splitting and binding energies, within experimental errors in referencing, and also gave unity intensity ratio. The third, lowest binding energy peak observed in the N 1*s* spectrum following exposure to NO at temperatures below 100 K was observed at 402.6 eV. For reasons described below this peak is attributed to a molecular, negatively charged, form of NO present upon the surface, denoted as NO^-.

Following exposure at 145 K the N 1*s* spectrum is dominated by a single peak, which is at the same energy (within 0.3 eV) as the peak observed at 100 K, and is therefore identified with the same NO^- species. Small amounts of N_2O are also observed along with another state designated as N_β. The amount of NO^- obtained upon the surface depends sensitively upon the initial oxidation state of the surface and also upon exposure as will be discussed below.

Exposure at 400 K gives rise to a different state observed at 6.1 ± 0.1 eV lower binding energy (396.5 eV) than the molecular NO^- species. This large shift suggests that this species is due to a negatively charged atomic N, i.e., a nitride N^{3-}. Additional evidence that this state is nitride-like was obtained from NO exposure to metallic Ce where nitride formation might be expected. In this case adsorption of NO on sputter cleaned Ce foil, followed by annealing to 700 K yields a single state in the N 1*s* and O 1*s* spectra which is assumed to result from dissociation of the NO. The binding energy of this N 1*s* state was measured at 396.7 eV, referenced to the Fermi edge observed from the Ce foil.

Exposure at 250, 300, and 350 K gave results intermediate between those at 400 K and at 145 K. Peaks due to the molecular NO^- and the N^{3-} states were present but the intensity ratio, NO^-/N^{3-}, decreased with increasing temperature of exposure. The ratio also varied somewhat from dose to dose. Some variation was possibly due to the degree of reduction of the initial ceria surface. At 250 K this ratio ranged from 0.4 to 0.6 for three different doses on surfaces with $f^{4+} = 0.25$, and 1.05 for a surface with $f^{4+} = 0.03$. At 300 K this ratio varied from 0.08 to 0.17, with no *systematic* variation with oxidation state detectable. In addition to N^{3-} and NO^-, two weaker peaks at intermediate energies, designated as N_α and N_β states, were also observed. The N_β peak was generally more intense than the N_α peak, but the relative intensities of N_α and N_β compared to those of N^{3-} and NO^- varied somewhat from dose to dose. Their relative intensities appeared to be affected by exposure, adsorption temperature, the crystallographic orientation, and the oxidation state of the sample, but they varied in a manner that could not be directly correlated with any of these parameters.

A N 1*s* spectrum for NO adsorbed at 90 K on the clean Ru(0001) substrate is compared in Fig. 2 with a spectrum obtained for reduced ceria exposed to NO at 150 K. The N 1*s* binding energy for NO/Ru(0001) was obtained by

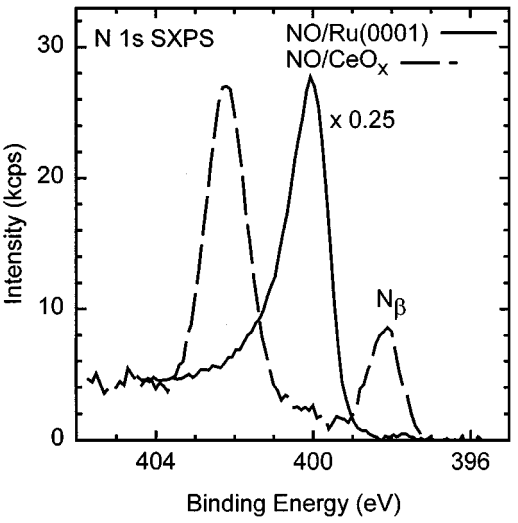

FIG. 2. N 1*s* SXPS spectra are compared for a 5 L NO exposure to a reduced ceria surface at 150 K (dashed curve) and for a clean Ru(0001) surface exposed to 20 L of NO at 88 K (solid curve). The ceria surface was 30% oxidized prior to NO exposure and 65% oxidized following the NO exposure.

referencing to the Fermi edge measured from the Ru surface, yielding a value of 400.0 eV in agreement with results of Umbach *et al.* (31). Referenced in this way, it is seen that the NO^-/ceria lies at a higher binding energy than for NO/Ru. Comparing intensities in Fig. 2 it is apparent that the reduced ceria can take up as much as 25% of the saturation NO coverage on the Ru surface. The saturation coverage for NO on Ru(0001) is 0.75 ML, corresponding to 1.2×10^{15} cm^{-2} (31, 32). The density of NO^- on the ceria is therefore on the order of 3×10^{14} cm^{-2} or about 0.36 molecules per Ce cation in the $CeO_2(111)$ unit cell. The spectrum shown in Fig. 2 corresponds to the largest peak intensity observed for a sequence of NO exposures at this temperature. The NO on Ru is also saturated since exposure to 40 L did not increase the intensity of the N peaks compared to 20 L exposure. A source of uncertainty is that the intensity of this NO^- state on ceria is highly sensitive to X-ray exposure (see below).

These results of NO adsorption were comparable for the different CeO_2 surfaces. This is illustrated in Fig. 3, which shows representative spectra for NO exposure at 300 K on four different surfaces. It is seen that the same four states are observed corresponding to N^{3-} and NO^- at the lowest and highest binding energies respectively with N_α and N_β at intermediate energies. The distributions of these states varies between samples with the (100) surface having slightly higher $NO : N^{3-}$ ratio than the (111) surface or the reduced ceria grown on Ce. It is seen that the N_α state was more prominent on the polycrystalline ceria grown by oxidation of Ce metal. In addition, this sample exhibited another weak feature at a binding energy higher than the NO^- feature. Adsorption on the $CeO_2(111)$/Ru thin films

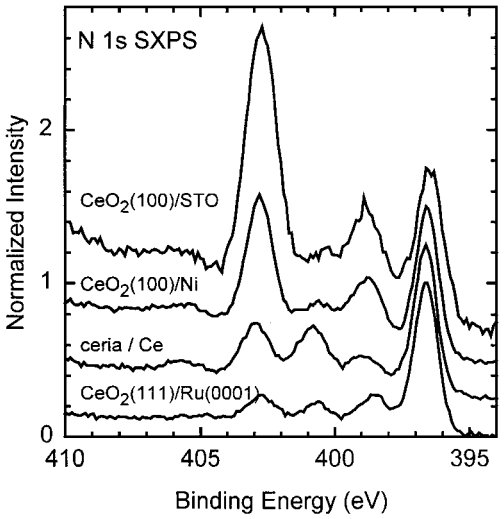

FIG. 3. N 1*s* SXPS are shown for adsorption of NO at 300 K on four types of samples. Each sample surface was reduced prior to NO exposure at 300 K. The spectra were obtained using different photon energies ranging from 520 to 600 eV and slightly different procedures were used to reference the binding energy scales. After these procedures the N^{3-} peak, shown at 396.6 eV, aligned to within 0.4 eV for all samples. For display purposes, the energy scales were shifted this remaining amount to align this peak in each spectrum. The intensity scales were normalized to unity intensity of this peak for each spectrum.

and the $CeO_2(100)$/Ni gave comparable results for exposure at 100 K (not shown), yielding strong NO^- and N_2O peaks, and occasional smaller amounts of N_β. Results for the $CeO_2(100)$/STO could not be checked at temperatures below 300 K, because sample charging was a serious problem at low temperatures for this sample.

Studies were performed to determine how the extent of the reduction of the ceria affected the adsorption of NO. The most extensive data was obtained for the $CeO_2(111)$/Ru sample since the degree of reduction could be systematically varied and was stable to high temperature anneals. For adsorption at 100 K, N_2O is always observed as an adsorption product. However, the relative proportion of NO^- to N_2O was found to be quite variable, ranging from 0.7 to 2.5. We were unable to correlate this variation with the extent of reduction of the surface measured prior to adsorption, indicating that this parameter did not completely control this ratio. Various other differences in the distribution of N states were observed which depend upon how reduced the surface was prior to adsorption. For adsorption near 150 K, a highly reduced surface, such as in Fig. 1 which was 6% oxidized before dosing NO, yields a small amount of N_β. Also, a small amount of N_2O is observed. Dosing a more oxidized surface resulted in much less uptake of NO, and relatively less N_2O and atomic N. It is expected that the relative amounts of these species depends sensitively upon the adsorption temperature and details of experimental procedure, due in part to high desorption rates of N_2O at this temperature. Since the sample was cooled after dosing with NO the details of how long the sample was at dosing temperature following termination of the dose may also affect the amount of N_2O observed.

A highly oxidized surface was generally less active for NO uptake than a reduced surface. There was NO uptake when exposure was performed at 100 K but different N 1*s* states are observed. This is illustrated in Fig. 4 which compares NO adsorption at 100 K on a fully oxidized and a sputter reduced $CeO_2(100)$. It is seen that the NO^- peak is much smaller on the fully oxidized surface and that in both cases N_2O is formed as indicated by the peak at 408 eV. However, on the oxidized surface, the second N_2O peak expected near 404 eV is overshadowed by a larger peak positioned at 1.1 eV higher binding energy. This situation is indicated by the spectral decomposition shown in the bottom part of Fig. 4. We attribute this new peak, observed on the fully oxidized surface to nitrite. Annealing this surface to 150 K results in desorption of the N_2O leaving only the nitrite feature with diminished intensity. Similar results were obtained for highly oxidized thin films of $CeO_2(111)$/Ru, indicating that these features occur on that surface also, although they were quite weak.

Additional information about the NO derived states was obtained from X-ray absorption measurements recorded at the N 1*s* edge and shown in Fig. 5. Results are shown for NO exposure at 150 K on a reduced ceria surface (top curve) and for NO exposure on an oxidized surface at 90 K followed by annealing to 150 K (bottom curve). These conditions were chosen to isolate and optimize the coverage of

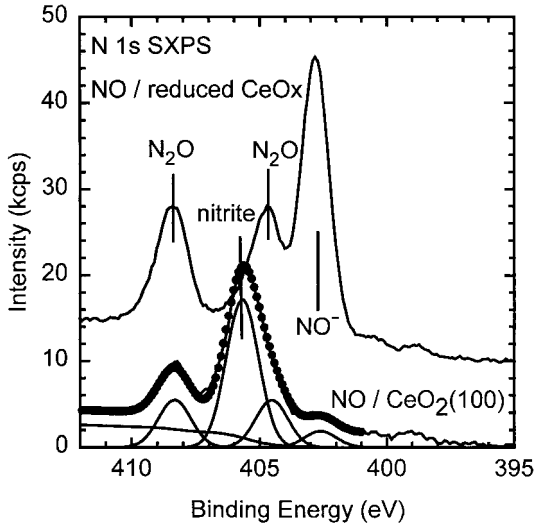

FIG. 4. N 1*s* SXPS are shown for adsorption of NO at 100 K on a fully oxidized (bottom) and a sputter reduced surface (top) for the $CeO_2(100)$/Ni thick film. The bottom spectrum was fitted with two N_2O peaks, an NO^- peak, a higher binding energy nitrite peak, and a Shirley type background [45] with the constraint that the N_2O peaks be of equal intensity and separated by 3.8 eV. The resulting fit is shown as points superimposed on the experimental spectrum.

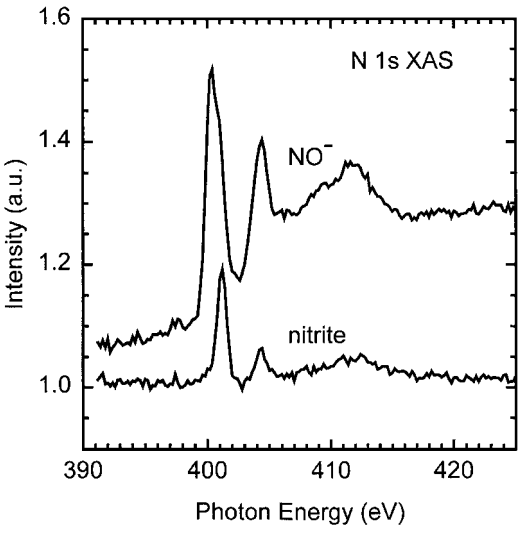

FIG. 5. X-ray absorption at the N K edge is shown for NO exposure on oxidized (bottom curve) and reduced (top curve) ceria. The reduced ceria film was grown on Ru and exposed to NO at 150 K, conditions which lead to formation of the state assigned to NO^-. A fully oxidized CeO_2(111)/Ru was exposed to NO at 90 K followed by annealing to 150 K to remove N_2O, conditions which lead to isolation of the state assigned to nitrite. The X-rays were incident along the surface normal. The signal from the partial yield detector was normalized by the incident X-ray flux.

features associated with NO^- and nitrite on the reduced and oxidized surfaces, respectively. It is seen that in both cases peaks are observed near 400 and 404 eV. Based upon previous analysis of NO photoabsorption (34) these peaks can be associated with the presence of π symmetry orbitals on the N atom, confirming the molecular nature of both species.

Adsorption of NO on a reduced surface always resulted in its reoxidation. This is illustrated in Fig. 6, which shows the Ce 4*d* spectrum before and after adsorption of NO at 300 K on an initially reduced ultrathin film of CeO_2(111). Prior to NO adsorption the ceria film was annealed to 900 K after which f^{4+} was estimated from curve "a" in Fig. 6 to be about 0.07, as indicated by the presence of the *D* peak and the very small X''' peak. Adsorption of NO at 300 K on this surface yielded curve "b" in Fig. 6, exhibiting an increase of X''' and decrease of *D* corresponding to $f^{4+} = 0.50$. This NO induced oxidation of the surface occurred at all temperatures even as low as 100 K where only the N_2O and NO^- peaks are observed in the N 1*s* spectrum. The amount of oxidation caused by a fixed 20 L dose of NO depended upon the initial degree of reduction and the temperature of adsorption. Generally, a greater change in oxidation state was observed for surfaces which were more highly reduced prior to NO adsorption. Also, a generally greater change in oxidation state was observed for highly reduced surfaces when the adsorption was performed at 300 than when performed at 100 K. However, for surfaces initially partly oxidized, no clear trend was discerned as the adsorption temperature was varied.

Part of the oxidation of the thin films caused by NO was reversible. This is illustrated in Figs. 6b and 6c for NO adsorption on a reduced ceria film grown on Ru(0001). Annealing the surface exposed to NO at 300 K through a sequence of short anneals at increasing temperatures up to 500 K reduced f^{4+} from 50 to 15%. Some amount of reversibility was always observed on reduced films grown on Ru. This reversible oxidation was studied further by the observation of both the Ce 4*d* spectrum and the N 1*s* spectrum as functions of annealing temperature following NO exposure. In general it was found that the majority of reduction occurred upon annealing between 300 and 500 K. This temperature range did not strictly correlate with loss of features in the N 1*s* photoemission spectrum. For adsorption at 100 K, the reduction occurred above the temperature at which most or all N containing species had already desorbed from the surface. The reversible oxidation was therefore mostly associated with oxygen migration. Reversible oxidation was not observed on the thick, sputter reduced CeO_2(111)/Ni films.

Continuous exposure to the X-ray beam induced changes in the N 1*s* spectra, in particular it caused decreases of the NO^- and N_2O intensities. There was evidence that loss of NO^- and N_2O was accompanied by growth of N_α. There was also evidence that the N^{3-} state also decreased with X-ray exposure with some amount of formation of the N_β state. There was no evidence that N_α or N_β decreased with X-ray exposures comparable to that used for analysis. In the absence of the X-ray beam the N_2O states were stable at 100 K and the NO^- state was stable at higher temperatures. Evidently the X-ray induces desorption and possibly some decomposition of NO^- and N_2O.

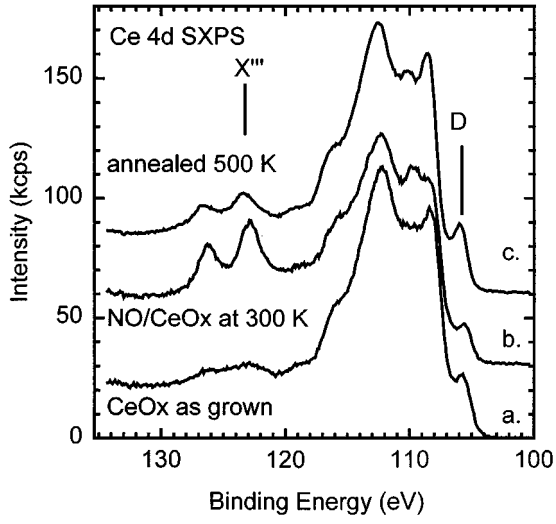

FIG. 6. Ce 4*d* photoemission spectra are shown for (a) highly reduced CeO_x as grown, (b) following NO adsorption on this surface at 300 K, and (c) following a 60-s anneal of the sample in (b). Changes in the X''' peak indicate oxidation by NO followed by reduction caused by annealing.

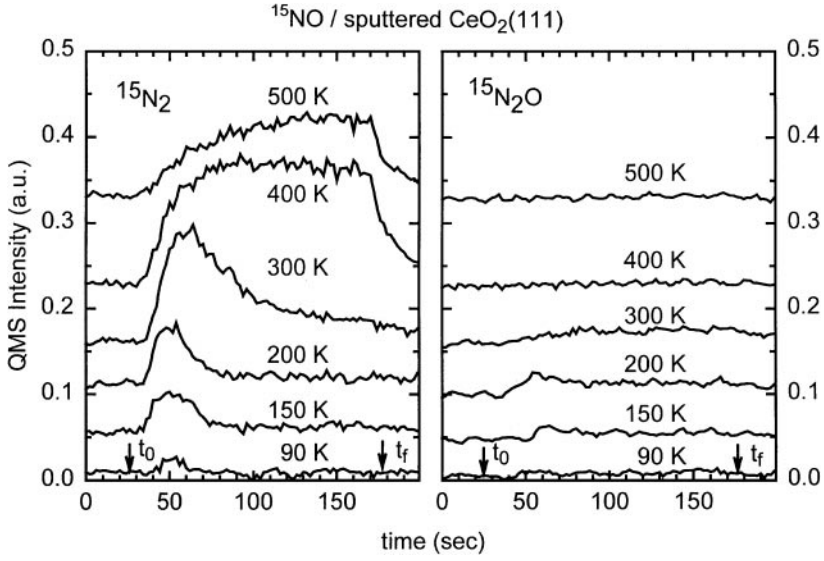

FIG. 7. Time profiles show the evolution of gas phase $^{15}N_2$ (left) and of gas phase $^{15}N_2O$ (right) as indicated by changes in the mass 30 and mass 46 signals during isothermal ^{15}NO adsorption. Results are shown at the indicated adsorption temperatures. Exposure is initiated at time t_0 and the exposure is quenched at time t_f.

3.2. Desorption Species Formed during Isothermal Adsorption

Some of the reaction products formed during NO adsorption desorb rapidly from the ceria surface at the adsorption temperature. This results in observable increases in ambient partial pressures during directed dosing. This is illustrated in Fig. 7, which shows the time profile of mass 30, $^{15}N_2$, and of mass 46, $^{15}N_2O$, during ^{15}NO isothermal exposure of a sputter reduced $CeO_2(111)$/Ni surface, recorded at various exposure temperatures. The ^{15}NO source valve was opened at time t_0 (between 20 and 25 s), which immediately starts the exposure. At a time t_f (near 175 s) pumping of the ^{15}NO ballast volume behind the aperture was initiated, effectively stopping the ^{15}NO exposure. The ballast pressure was the same in each exposure to within 5% so the rate of exposure should be comparable in each case. The exposure rate was estimated to be 0.01 L/s. Each curve corresponds to exposure to a freshly sputtered surface and so to a highly reduced surface. However, at the higher temperature, oxygen migration between the bulk and the surface may occur during the dosing. The $^{15}N_2$ time profiles shown on the left side in Fig. 7 were corrected for an interference between product $^{15}N_2$ and ^{14}NO impurities, present in the ^{15}NO source at a level of about 3%. This interference was removed by correcting the mass 30 profiles by the simultaneously measured profile for ^{15}NO (mass 31).

Summarizing the data in Fig. 7, there is clear evidence of $^{15}N_2$ desorption at all temperatures of 150 K or above for the sputter reduced $CeO_2(111)$. The maximum rate of $^{15}N_2$ evolution appears to be achieved at adsorption temperatures of around 400 K. A small amount of $^{15}N_2O$ is evolved between 150 and 300 K but is not detected during adsorption at 400 or 500 K. On the fully oxidized surface, no $^{15}N_2$ or $^{15}N_2O$ could be detected, above background level, for any temperature.

These results indicate that NO dissociation occurs at low temperatures on the sputter reduced surface, and some product N_2 is immediately desorbed. Desorption of product N_2O at 150 K indicates that the mechanisms leading to surface N_2O, observed by photemission at 100 K, occur at higher temperatures on both surfaces. The N_2O species must desorb as soon as it is formed when the sample temperature is above the temperature programmed desorption temperature of about 140 K. When adsorptions are performed above 200 K, production of N_2O diminishes due to competition with the production of N_2. At sufficiently high temperatures the rate of N_2 production also diminishes. This is probably a result of oxygen diffusion to the surface, causing surface oxidation and inhibition of NO uptake and dissociation.

3.3. Surface Species Formed with Increasing Temperature

The evolution of the N 1*s* states with temperature was studied by performing short anneals to sequentially higher temperatures, following adsorption at various temperatures. A fixed exposure of 20 L was used to dose the surface. The evolution following adsorption at 100 K is shown in Fig. 8. These measurements were obtained from a sputter reduced $CeO_2(100)$, but similar results were obtained on reduced ultrathin $CeO_2(111)$.

For adsorption at 100 K the spectrum exhibits states associated with N_2O and NO^-. Annealing to 145 K causes a decrease of the NO^- intensity and especially the N_2O states. It was observed that N_2O was desorbed during this anneal.

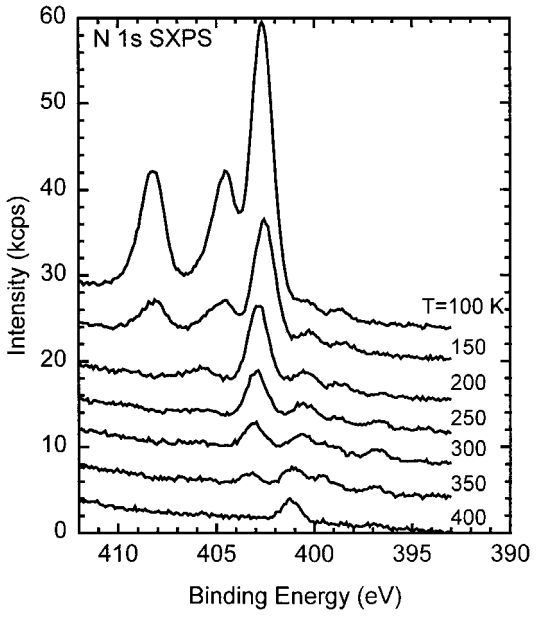

FIG. 8. Evolution of the N 1*s* photoemission as a result of sequential 30 *s* anneals at increasing temperatures. Initially the CeO_2(100)/Ni surface was about 5–10% oxidized before exposure to 20 L of NO at 100 K and was 60 to 65% oxidized following exposure.

There may also have been NO evolved, but due to interference from the cracking fragment of N_2O this was not certain. Annealing to higher temperatures further decreased the surface NO^-, with 70% gone by 200 K and complete loss by 400 K. Some of this loss may occur due to reaction to produce desorbing N_2O. Annealing to 200 K reveals a small amount of the feature associated with nitrite present on the surface which may have been present at lower temperatures, as indicated by a shoulder on the (lower binding energy) N_2O peak. The nitrite feature was weak for this reduced surface but was much more pronounced on oxidized CeO_2(100), where it persisted upon annealing to 350 K and on oxidized CeO_2(111), where it persisted to above 200 K. It was not convincingly seen on highly reduced CeO_2(111). N_α, N_β, or N^{3-} do not grow as a result of annealing, indicating no appreciable thermal conversion of either the N_2O or the NO^- into these states. N_β remains up to about 300 K, and N_α persists to 400 K or higher.

For adsorption at 250 K, as seen in Fig. 1, the spectrum exhibits three states: NO^-, N_β, and N^{3-}. Annealing a surface exposed at 250 to 300 K for 30 s eliminates almost all of the NO^- and the N_β states, while the N^{3-} state remains nearly undiminished (not shown). Further annealing to 350 K leads to complete loss of remaining NO^- and attenuation of N^{3-}. The N^{3-} completely disappears following annealing at 500 K. Small amounts of the N_α state are occasionally observed following adsorption at 250 K, and if present it persists to temperatures above 600 K.

For adsorption at 300 K, as seen in Fig. 1, the spectrum exhibits mostly N^{3-} and small amounts of NO^-, N_α, and N_β. Annealing to 350 K leads to complete loss of remaining NO^-, a decrease in N_α and N_β, and some decrease in N^{3-} (not shown). Annealing to 500 K leads to nearly complete loss of N^{3-} and once again a small amount of N_α persists.

On the fully oxidized surface only nitrite and N_2O are present following exposure at 100 K (Fig. 4). Annealing to 150 K results in loss of most or all N_2O, as on the reduced surfaces. A portion of the nitrite remains. Annealing to higher temperatures causes further loss of the nitrite, with some persisting to temperatures as high as 300 K (not shown).

3.4. Desorption Species Formed with Increasing Temperature

Temperature programmed desorption (TPD) studies were conducted on the thick CeO_2(111)/Ni films and on thin CeO_2 (111)/Ru following adsorption of ^{15}NO. TPD curves for CeO_2(111)/Ru are illustrated in Fig. 9. An experimental difficulty in quantifying the TPD was distinguishing desorption from the ceria surface and background desorption originating from the back of the Ru (Ni) substrate, from the thermocouple and from the W support leads. Various steps were taken to reduce background including the use of a directed NO dosing of the front surface, sulfidation of the back of the Ru crystal, and preflashing of the sample wires prior to TPD. Blank exposures were conducted in which

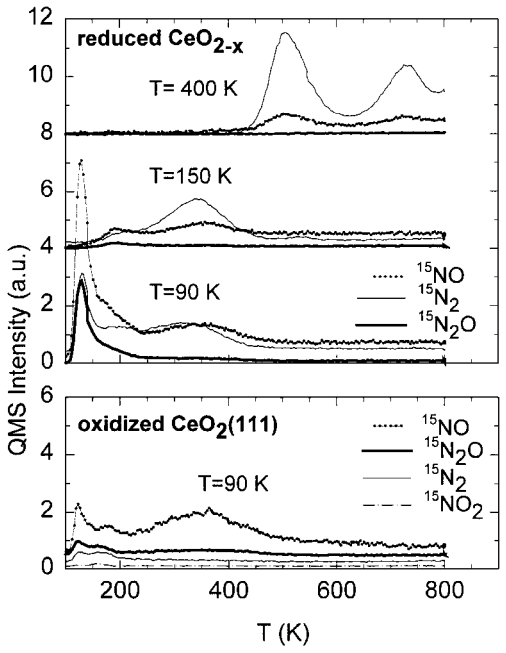

FIG. 9. Desorption profiles are shown during linear temperature increase for various masses and following exposure to ^{15}NO at indicated temperatures. Results are shown for a fully oxidized (bottom) and for a sputter reduced (top) CeO_2(111)/Ru surface. Each desorption curve is corrected by subtracting background desorption from a blank exposure (see text). Data are shown for ^{15}NO (mass 31), $^{15}N_2$ (mass 30), $^{15}N_2O$ (mass 46), and $^{15}NO_2$ (mass 47).

^{15}NO was released through the directed doser but without placing the sample in the dosing position. Such exposure should simulate exposures on the back surface comparable to those during directed dosing, but with substantially less exposure on the front surface compared to directed dosing. The TPD spectra shown in Fig. 9 were corrrected by subtracting the desorption observed following blank exposures. Except for differences in details due mostly to the background problems, both samples yielded qualitatively consistent results and conclusions.

The TPD profiles observed from a sputter reduced surface are shown in the top panel of Fig. 9. $^{15}N_2O$, ^{15}NO, and $^{15}N_2$ are desorbed following adsorption at 90 K, most in a low temperature peak below 200 K. Although little or no $^{15}N_2O$ desorbs following exposures at 150 K or above, there is pronounced tail at high temperatures between 150 and 200 K following adsorption at 90 K, indicative of reaction limited N_2O production. There is clear evidence for $^{15}N_2$ evolution from the reduced surface, discernable in peaks at various temperatures. Following adsorption at 150 K, TPD yields dominantly $^{15}N_2$ and lesser amounts of ^{15}NO, even though the SXPS reveals that mostly $^{15}NO^-$ is present upon the surface (Fig. 1). Evidently the $^{15}NO^-$ dissociation and recombination of resultant ^{15}N is favored compared to its desorption as ^{15}NO. Following adsorption at 400 K, $^{15}N_2$ desorption occurs in two peaks not seen for lower adsorption temperatures. These two peaks may be associated with recombination of surface and bulk nitride states, the bulk component limited by diffusion and therefore appearing at a higher temperature. (Fig. 9). There is relatively less ^{15}NO desorption following adsorption at 400 K, but it correlates with the $^{15}N_2$ desorption, indicating NO formation by N and O recombination.

The TPD profiles observed from an oxidized surface following adsorption at 90 K are shown in the bottom panel of Fig. 9. Mass 46 profile indicates desorption of $^{15}N_2O$ in a double peak below 180 K. The $^{15}N_2$ profile, mass 30, mimics the $^{15}N_2O$ profile. A small portion of this peak is expected to be due to impurity ^{14}NO desorbing with the ^{15}NO (3% of the ^{15}NO peak) and $^{15}N_2$ cracking fraction from the $^{15}N_2O$ desorption (9% of the $^{15}N_2O$ peak). The ^{15}NO profile, mass 31, also mimics the $^{15}N_2O$ profile below 180 K, and shows a broad desorption occurring between 200 and 450 K. The low temperature peak is due in part to cracking fraction of $^{15}N_2O$ (33% of the $^{15}N_2O$ peak). ^{15}NO is the dominant desorption channel following 90 K exposure. Due to imperfect background correction, it was not possible to prove that the ^{15}NO desorption in the range of 200 to 400 K originates from the ceria and not from the background desorption. Similarly, it is difficult to show conclusively that there are any desorption products from ceria following exposures at 150 K or above. However, SXPS shows that small amounts of nitrite persist on the surface following adsorption at 90 K and subsequent anneals to temperatures up to 300 K, so some desorption of N containing products must occur in this range. Also, no uptake of NO was detected by SXPS on the oxidized surface following adsorption at 150 K.

3.5. *Exposure Dependence in Isothermal Adsorption*

The evolution of the N 1*s* spectra with NO exposure at 90 K yields information about the growth of the N_2O, as shown in Fig. 10 for a sputter reduced ceria. At lowest exposure, molecular NO^- and various atomic N states are observed, with the most prominent state being N_β. In particular there is no sign of N_2O, which appears only after 4 L. NO^- and N_2O grow at the expense of N_β and N^{3-} which decrease as exposure increases. Typical measurements in which a sample was exposed to 20 L in a single dose lead to a surface with principally NO^- and N_2O present, and amounts of N_α, N_β, and N^{3-} usually smaller than shown in Fig. 10. On the CeO_2(111)/Ru surface, many of the same trends are observed that are shown in Fig. 10. In particular N_β and NO^- are dominant at low exposures, and N_2O is small, while increasing coverage causes N_β to diminish while N_2O grows. High exposures led to N_2O and NO^- only.

At higher temperatures, the exposure dependence reveals an unusual effect of the reactive adsorption of NO. This is illustrated in Fig. 11 which shows the results of sequential exposures at 400 K on highly reduced CeO_2(111). A 1 L exposure at 400 K leads exclusively to the N^{3-} state. With increasing exposures the N^{3-} state grows in intensity

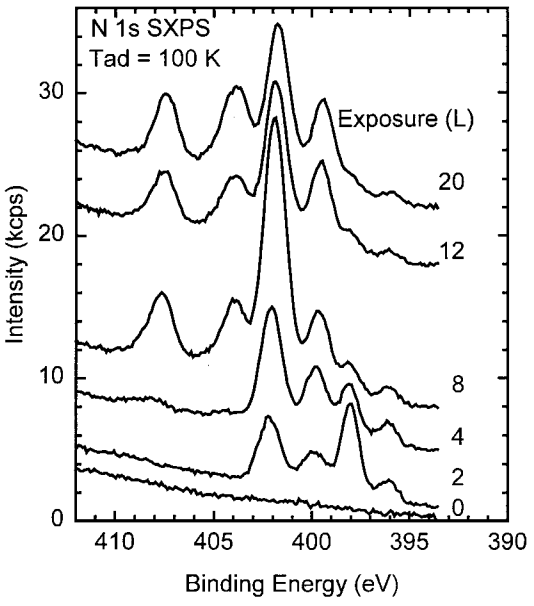

FIG. 10. N 1*s* photoemission spectrum is shown as a function of NO exposures to a sputter reduced CeO_2(100)/Ni surface. These spectra were obtained following a sequence of increasing NO exposures at an adsorption temperature of 100 to 105 K. The accumulative exposure is shown. The surface was initially 0% oxidized (all Ce^{3+}) prior to the first exposure and was about 50% oxidized following the last exposure.

until the range of 20 to 40 L at which point further exposure causes a decrease in the N^{3-} signal. Exposure to 130 L finally yields less N^{3-} than was present after the initial 1 L exposure. Throughout the exposures the N_β state continues to grow. Additional tests proved that the N^{3-} is thermally stable at 400 K and that X-ray exposure was not responsible for the observed decrease in N^{3-}, although it may be partly responsible for the growth of N_β seen in Fig. 11. Measurement of the valence band spectra showed that the NO substantially oxidized the sample with f^{4+} changing from 0.0 to 0.90 after the last exposure. Consistent with results given above, as the increasing NO exposure oxidizes the surface, the stable coverage of resulting N^{3-} decreases due to its oxidation and recombination. This displacement by NO is responsible for a maximum in the N^{3-} coverage vs exposure relationship.

A similar behavior is observed for adsorption at 150 K. At this adsorption temperature NO^- is the primary surface species (Fig. 1), although the N_β peak is observed at low exposures. High exposures at this temperature ultimately leads to a decrease of both the N_β and the NO^- peaks, similar to the loss of N^{3-} observed for 400 K adsorption. However, the NO^- state is extremely sensitive to X-ray irradiation, making it difficult to determine an accurate exposure dependence.

3.6. N_2O Adsorption Studies

Adsorption of N_2O on sputter reduced ceria at 90 K yields the characteristic two peaks attributed to N_2O in the N 1*s*

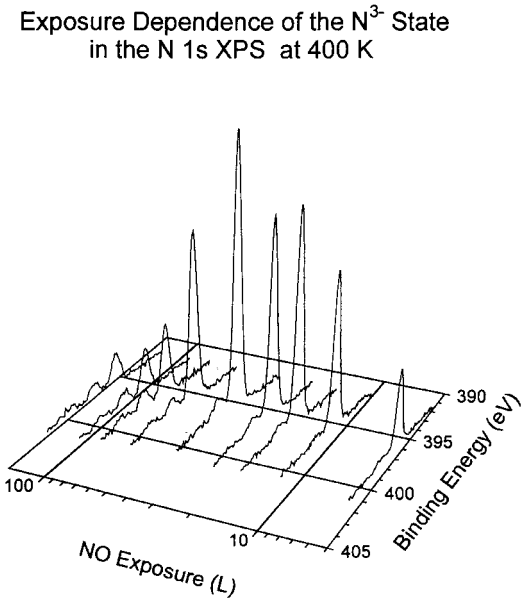

FIG. 11. As in Fig. 10 except the sample was CeO_2(111)/Ru film and the adsorption temperature was 400 K, resulting principally in the N^{3-} state. The surface was initially 0% (all Ce^{3+}) oxidized prior to the first exposure and was about 87% oxidized following the last exposure.

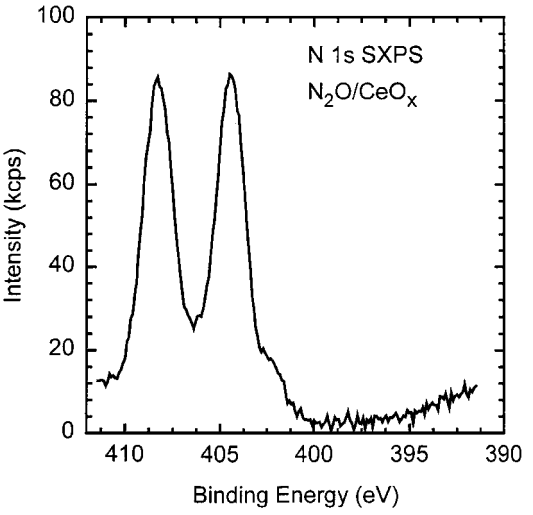

FIG. 12. N 1*s* SXPS are shown for adsorption of N_2O at 100 K on a sputter reduced surface for the CeO_2(100)/Ni thick film.

SXPS (Fig. 12). Adsorption does not give rise to observable atomic N peaks in the N 1*s* spectrum, but a shoulder with intensity of about 20% of the intensity of the N_2O peaks was observed at the binding energy associated with the NO^- state. This implies that some N_2O may react to form NO^-, but it does not appear to produce stable surface N in the process. Formation of NO^- evidently results from direct decomposition or reaction between N_2O molecules with direct formation and evolution of N_2. Alternatively, N atoms once formed may immediately react with N_2O or NO to form and desorb as N_2. N_2 is evolved during isothermal N_2O exposure at 90 K, confirming its immediate formation from N_2O reaction on a sputter reduced ceria (not shown). Adsorbed N_2O is cleanly desorbed by heating to 150 K without leaving N-containing species on the surface. N_2 is also evolved, indicating competition between desorption and reaction.

4. DISCUSSION

4.1. Identification of Surface Species

Assignment of the N 1*s* spectra is based upon the qualitative trend that the observed binding energy increases with the formal valence state of the nitrogen. The range of binding energies observed in previous studies of inorganic solids indicate a range in N 1*s* binding energies from about 396.6 to 397.2 for nitrides (of Cr, V, and W) up to 407.4 eV for sodium nitrate, i.e., a range of about 10.8 eV for a valence state range of 8 units (from N^{3-} to N^{5+}) or about 1.3 eV per oxidation state (35–38). In the present study a range of 11.9 eV is observed between peaks with the lowest and the highest binding energies.

The peak at 396.5 eV appears to be nitride-like, i.e., N^{3-}, based upon its binding energy and from comparison

with NO adsorption on Ce metal. X-ray absorption of this species is similar to that seen for TiN (8). Formation of this product requires that the ceria be highly reduced. Dissociation of NO into a nitride and O^{2-} requires transfer of five electrons to the molecule requiring five adjacent Ce^{3+} cations or possibly lower oxidation states or metallic Ce. Metallic Ce could be detected by appearance of a Fermi edge which was occasionally detected after certain film preparations. However, the N^{3-} peak was observed even when no such edge was evident.

The assignment of the N_2O peaks are well proven from various evidence. The measured 3.8-eV splitting fits well to the 3.7 eV in the gas phase (35) and 3.7 to 4.0 eV measured on other surfaces (Table 1). Other evidence includes the measured binding energies, correlation of both peak intensities upon annealing, prominent N_2O desorption product seen in TPD following adsorption at 100 K, and comparison with direct adsorption of N_2O. This weakly held species cannot be N_2 since the 3.8 eV splitting indicates substantially inequivalent N atoms. Physisorbed N_2 may have inequivalent N atoms due to the orientation of the molecule on the surface, as seen for N_2 adsorption on W(110) (39), but in that case the observed splitting, 1.3 eV, is smaller than we observe.

The peak observed near 402.6 eV (Fig. 1) is associated with an undissociated form of NO. There may be charge transfer with the oxide upon adsorption to form a charged species, i.e., NO^+ or NO^-, or there may be dimerization occurring. Based upon experimental gas phase measurements the binding energy of the N atom in NO should be intermediate between those of the inequivalent N atoms in N_2O (35). In the present case the peak is observed at lower binding energy than either of the N_2O peaks, which might suggest that it is due instead to NO^-. Contrasting this is the fact that the peak position is higher than that of molecular NO adsorbed on Ru (Fig. 2 and Table 2), suggesting that it is NO^+. However, due to differences in shielding, relaxation, and the uncertainties in referencing, this latter comparison is probably not reliable. Literature results given in Table 1 indicate that the N in NO may have a binding energy which is larger, about the same or smaller than that of the lower peak of N_2O adsorbed on the same surface. These cases may illustrate variable extent of charge transfer to the NO.

Since this species is seen prominently on reduced ceria and only weakly on oxidized ceria (Fig. 4), it is presumably adsorbed at a Ce^{3+} site. In this case, transfer of an electron from the Ce 4*f* to NO could lead to NO^-, which is expected to weaken the NO bond, leading to a high probability of decomposition or to N_2O formation. The observed gas phase products are consistent with this conclusion. The isothermal adsorptions yield N_2 at temperatures of 150 K or higher on sputter reduced CeO_2(111) and CeO_2(100) surfaces. Following adsorption at 150 K the NO^- is the predominent surface species with very little dissociated N present (Fig. 1), yet during subsequent TPD there is more N_2 desorbed than NO (Fig. 9). This indicates that dissociation of the species competes with its desorption, consistent with its identification as the anion, NO^-.

Adsorption of NO at 100 K on a completely oxidized surface leads to a state observed at 405.7 eV (Fig. 4). Since its binding energy is higher than that of NO^- it is associated with a more positively charged form of N. Possible species include neutral NO, NO^+, nitrite, or nitrate. The binding energy is intermediate between the N_2O peaks, as found for the binding energies in gas phase N_2O and NO. However, for the surface species the binding energy is 3.1 eV lower than NO^-, suggesting a change of two oxidation states, more consistent with NO_2^- or NO^+ than for NO. Also, we can eliminate radical NO as a possibility. It is known from EPR results that, although radical NO adsorbs at 77 K on oxidized ceria, this species is very weakly held and is observed only in the presence of gaseous NO, conditions not met in our measurements (21). Formation of NO^+ would require electron transfer from the NO to an oxidized CeO_2 surface. This would not occur at uncoordinatively saturated Ce^{4+} states, creating a Ce^{3+}, since the reverse transfer occurs when NO is adsorbed on a Ce^{3+} cation. Consistent with this, we see no evidence in the photoemission for formation of Ce^{3+} resulting from this adsorption. Therefore, the most likely explanation is that the NO reacts to form a nitrite type species, NO_2, NO_2^-, or $NO_2^=$. This may occur either by bonding at a terminal $O^=$ or by a disproportionation reaction between NO molecules, a mechanism which would also explain the observed N_2O formation. In the latter case, N_2O formation might occur by NO dimerization and reaction leading to free or active oxygen which quickly reacts with physisorbed NO to form NO_2. NO_2 resulting from this disproportionation, involving three NO molecules, is not observed on the reduced surface because the O atoms rapidly react with the reduced Ce sites, inhibiting formation of the nitrite. Although we cannot specify the charge state with certainty, the observed binding energy is most consistent with an NO_2^- species. In TPD following exposure, NO is the predominent desorption species and little or no NO_2 is observed (Fig. 9), indicating that decomposition is favored over desorption.

Assignments of the N_α, N_β peaks are uncertain, since they were weak and difficult to isolate. They are less prominent than the nitride, NO or N_2O states. Their relative intensities were difficult to reproduce and varied from surface to surface. At 100 K, N_β is observed at low exposures prior to formation of N_2O at higher exposures. During increasing exposure at 150 K, the N_β peak grows in prior to NO^- and then is displaced by it at higher exposures. N_α and N_β states appear to result in part from X-ray irradiation of N^{3-} (N_β) or of NO (N_α). They were occasionally observed to grow from thermal conversion of the N^{3-} state at very high temperatures. Because of the progression of their binding

energies, it is tempting to assign the N_α and N_β states to N^{2-} and N^- type states, suggesting possibly –NH and $–NH_2$ species resulting from adventitious hydrogen. The presence of such H occurred especially after long cooling at low temperatures as indicated by an OH^- peak observed in O 1*s* photoemission (29). However, the N_α and N_β states were frequently observed when no OH^- peak was present suggesting that this is not their origin. A better explanation is that they are due to dissociated forms of N such as anionic N bonded to cationic sites and defect sites. This suggests instead that N_β is a decomposition product (i.e., atomic or anionic N) which readily recombines to evolve N_2 or reacts with NO^- to form N_2O. Different local environments result in different amounts of charge transfer to the N atoms and therefore different binding energies. The local availability of Ce^{3+} cations for charge transfer may control the relative amounts of N_α, N_β, and N^{3-}. The difficulty of controlling such sites may be responsible for the difficulty in reproducing the relative intensities of N_α and N_β.

Previous spectroscopic identification of surface species following NO adsorption on ceria has been carried out by FTIR and by EPR (18, 20–22). In these studies the presence of Ce^{3+} could not be generally confirmed or quantified as in the present study. On surfaces assumed to be partially reduced, the principle species observed are nitrosyls, nitrites, and hyponitrites formed from dimerization of the NO. The nitrosyl probably corresponds to the species identified as NO^- observed in the present study. This species, characterized by a band at 1165 to 1175 cm^{-1} is dominant in the FTIR spectrum at 298 K for all samples including those believed to have the most oxygen vacancies. There do not appear to be FTIR measurements at low temperatures to confirm that the NO^- also exists at 150 K where we see it most prominently in SXPS.

FTIR yields evidence for hyponitrite $(N_2O_2)^{2-}$, resulting from NO dimerizing at Ce^{3+} sites (22). Based upon the charge on the N, it may be expected that $(N_2O_2)^{2-}$ would appear at the same binding energy as NO^- and thus be indistinguishable by photoemission. Matinez-Arias *et al*. suggest that NO^- dimerizes to form hyponitrite which then decomposes by slow N–O bond cleavage to form N_2O. The NO^- and dimerized hyponitrite feature seen in the FTIR are believed to be the precursor for N_2O formation. In the present results the N_β is seen to form prior to N_2O species and then diminish as N_2O is formed, implicating N_β as a precursor to N_2O formation. This result suggests that hyponitrite may not be the only precursor.

As summarized by Trovarelli (24), there is evidence that NO reacts with O^{2-} on the surface to form NO_2^-. According to Martinez-Arias *et al*., this reaction occurs at "low activation levels," i.e., on an oxidized surface (22). A mechanism for this adsorption, resulting in creation of vacancies and an increase in conductivity has been described (40, 20). The photoemission peak at 405.7 eV presumably corresponds to this species. Our results indicate that creation of this species is accompanied by formation of N_2O, suggesting that formation of this nitrite may occur by reaction not with the surface but between surface NO. As noted above, creation of this state occurs in the absence of any Ce^{3+} on the surface.

N_2O is seen at 298 K in the FTIR measurements of Martinez-Arias *et al*. This does not contradict the present observation that N_2O is not stable on the surface above 140 K. In the FTIR experiments, the presence of N_2O was explained as due to equilibrium uptake with N_2O in the ambient which contained product N_2O. Removal of the ambient caused loss of the N_2O signal.

4.2. Mechanisms of NO Reaction

Comparison of the surface species with the desorption products evolved during isothermal adsorption and during subsequent TPD suggest the following reaction pathways for the fully oxidized surface. Adsorption of NO at 100 K leads to surface N_2O and nitrite but little or no atomic or anionic N. If NO dissociation occurs, then the resulting N and O atoms must react rapidly with NO to form N_2O and NO_2. If NO dissociation does not occur then formation of NO_2 and N_2O implies direct reactions between three NO molecules. Increasing the surface temperature during TPD causes simultaneous desorption of N_2O, NO, and N_2 but no NO_2 evolves. Although it has previously been concluded that Ce^{3+} promotes N_2O formation (41), these results indicate that Ce^{3+} need not be present for N_2O formation. More detailed TPD data, including O_2 profiles and a means of decreasing background interference, are required to quantify the distribution of desorption products as a function of adsorption temperature.

For the reduced surface dissociation of NO occurs readily, although not completely, at low temperatures. The undissociated NO converts mostly to NO^- and N_2O. The occurrence of dissociation is evident from atomic or anionic N species observed in SXPS, from the N_2 evolution which occurs during adsorption (at least above 150 K), and from reoxidation of the ceria. Some NO^- does not dissociate following isothermal exposure at temperatures up to 300 K, and its rate of dissociation is competitive with its rate of desorption. This is indicated by subsequent TPD where N_2 and NO both evolve over a wide temperature range, although N_2 is the favored product. The different types of N atoms, N_α, N_β, and N^{3-} indicate site heterogeneity which may explain the wide temperature range of N_2 desorption, NO dissociation and NO desorption. The least stable N states recombine and desorb rapidly and therefore would not be seen by SXPS.

Data in Fig. 10 indicate that N_2O may form by reaction between N_β and NO. This hypothesis is suggested by the fact that the N_β population, which forms at low exposure, decreases at higher exposure. Simultaneously the population

of N_2O, which must form by reaction between at least two species, increases. Since N_β is thought to be atomic or anionic, reaction with NO^- is a plausible mechanism for N_2O formation. However, it cannot be proven that N_β is not simply displaced by NO^- or N_2O or that it reacts to form NO^-. In contrast, N_β is not seen on the oxidized surface, suggesting that N_2O forms by reaction between NO species. It is also possible that both processes occur on the reduced surface. A broad, weak desorption of N_2O above 150 K suggests that N_2O formation continues even though adsorbed N_2O is not visible by SXPS.

The formation of N^{3-} and its recombination to N_2 are thermally activated. The evidence is that this state does not form in high quantities unless exposure is performed near 400 K, even though NO dissociation occurs at lower temperatures as indicated by (i) reoxidation of the surface, (ii) the isothermal evolution of N_2 during adsorption, and (iii) subsequent N_2 desorption during TPD at temperatures below 400 K. In other words, the presence of N surface intermediates does not lead to N^{3-} unless the temperature is near 400 K. The recombination of N^{3-} to form N_2 occurs near 500 and 700 K, while N_2 evolution following NO^- dissociation occurs between 200 to 400 K. (Fig. 9). The cause of the activation of the 500 K peak may be the large number of electrons which must be accommodated to create N^{3-} from NO or to evolve N_2 from N^{3-} anions. Activation of N^{3-} bulk diffusion may be the cause of the 700 K peak.

4.3. Surface Oxidation by NO

The Ce 4*d* photoemission, illustrated in Fig. 6, indicates that a limited exposure of NO at any temperature causes a decrease in the fraction of Ce^{3+}. The isothermal evolution of N_2 during exposure also suggests decomposition of NO at a rate which increases with increasing temperature. Formation of N_2O, observable following adsorption at 100 K is another indication of dissociative adsorption of NO. Since much of the N is immediately desorbed, the N 1*s* SXPS observed following exposure at higher temperatures does not reveal the extent to which dissociative adsorption is occuring. Continued exposure to NO can lead to complete irreverisble oxidation of the ceria surface.

Oxidation of ceria by NO has been reported previously for Rh/CeO_2 catalysts (42). In that case, rapid reoxidation was observed at 300 K with evolution of N_2 and N_2O. In studies of dispersed titania, it has been found that high temperature reduction of preoxidized TiO_2 causes a loss of IR transparency due to the creation of free electrons (15). The major effect of room temperature exposure of reduced TiO_2 to NO is an increase in the IR transparency, associated with the loss of carriers from the titania (15). No NO vibrational features are observed. The loss of carriers is attributed to electron transfer to the O atoms resulting from dissociation of NO. Room temperature exposure to NO can completely restore the transparency of the sample to that of a sample pretreated in oxygen at 623 K. Similar results are obtained for ceria doped titania (23). Variation of transparency induced by NO adsorption is not mentioned in FTIR studies of NO reactions on ceria (20–22).

The reversibility of the ceria oxidation observed in Fig. 6 might have have several possible causes. The most likely cause is that the annealing to 500 K is sufficient to cause surface oxygen, resulting from the NO dissociation, to migrate into the reduced thin film, causing the apparent further reduction (decrease of Ce^{4+}) of the surface region observed by SXPS. This explanation is consistent with the fact that the reversible behavior observed in Fig. 6 is not observed on sputter reduced thick films, i.e., the $CeO_2(111)/Ni$ and $CeO_2(100)/Ni$, where outward oxygen migration from the fully oxidized bulk occurs near 500 K.

Other possible explanations of the reversible oxidation can be eliminated. One possibility is that a portion of the ceria oxidation caused by NO is brought about by the reduction of physisorbed NO in the formation of NO^-, effectively removing an electron from a Ce^{3+} ion. Upon desorption of NO, the electron would be transferred back to the solid reversing the redox process. Similarly, recombination of N^{3-} resulting in desorption of N_2 or recombination and desorption of any O^- or O_2^- species should result in an increase in Ce^{3+}. However, the measured values of f^{4+} did not correlate with the NO^- peak (or of the N_2O peaks) in the N 1*s* spectrum following adsorption at 100 K. Annealing to temperatures between 100 and 200 K yielded a large decrease in the surface coverage of the NO peak with little or no increase in the amount of Ce^{3+}. Therefore NO^- is not the primary reducing agent responsible for the reverse oxidation. In some cases where substantial reversible oxidation was observed, a large amount occurred upon annealing from 400 to 500 K, the temperature range where the N^{3-} state desorbs. However, this reversible reduction was also observed in this temperature range for surfaces which did not have substantial quantities of the N^{3-} state. In addition, no O_2 desorption was observed during this or any other temperature range. Therefore, although such electron transfer processes may occur they are not responsible for most of the reversible oxidation.

7. CONCLUSIONS

Interaction of NO with ceria depends upon temperature and oxidation state and to lesser extent upon the crystallographic orientation of the ceria. Oxidized surfaces do not adsorb NO above 150 K, but at 90 K NO adsorbs and reacts to form N_2O and nitrite on fully oxidized CeO_2. Reduced and sputter reduced surfaces, containing high concentrations of Ce^{3+} cations, are more reactive than fully oxidized surface. On reduced surfaces there is dissociation of NO, charge transfer to NO to form NO^- at coverages as high as 1/3 ML, and formation of N_2O partly by reaction between

NO (or NO^-) and atomic or anionic N. Exposure to N_2O also results in NO^-, indicating reversible reaction between N_2O and NO (or NO^-) on the surface. Various forms of N (N_α, N_β, and N^{3-}) are observed which are associated with adsorption at Ce cations, and the formation of N^{3-} indicates that as many as five Ce^{3+} cations may contribute to dissociation of an NO molecule. N_2 evolution (and some N_2O) is observed immediately upon NO exposure in amounts which increase with adsorption temperature, possibly indicating the formation of a reactive, atomic N intermediate. Dissociative adsorption of NO leads to the displacement of N^{3-} at high exposures. Oxidation of the reduced surface by NO occurs upon adsorption at 90 K implying nonactivated dissociation at some sites. Redistribution of Ce^{3+} cations occurs rapidly by 500 K, probably due to activated diffusion of oxygen. Certain N-containing states are sensitive to X-ray irradiation.

ACKNOWLEDGMENTS

We thank M. Paranthaman and D. P. Norton for providing CeO_2 samples. Research was sponsored by the Division of Chemical Sciences, Office of Science, U.S. Department of Energy, under Contract DE-AC05-96OR22464 with Oak Ridge National Laboratory, managed by Lockheed Martin Energy Research Corp. The National Synchrotron Light Source at Brookhaven National Laboratory is supported by the Division of Chemical Sciences and Divsion of Material Sciences of the U.S. Department of Energy under Contract DE-AC02-76CH00016.

REFERENCES

1. Taylor, K. C., *Catal. Rev. Sci. Eng.* **35**, 457 (1993).
2. Fisher, G. B., Theis, J. R., Casarella, M. V., and Mahan, S. T., SAE paper 931034, 1993.
3. Yao, H. C., and Yao, Y. F., *J. Catal.* **86**, 254 (1984).
4. Oh, S. H., and Eickel, C. C., *J. Catal.* **112**, 543 (1988).
5. Nunan, J. G., Robota, H. J., Cohnand, M. J., and Bradley, S. H., *J. Catal.* **133**, 309 (1992).
6. Stubenrauch, J., and Vohs, J. M., *Catal. Lett.* **47**, 21 (1997).
7. Bunluesin, T., Cordatos, H., and Gorte, R. J., *J. Catal.* **157**, 222 (1995).
8. Overbury, S. H., Huntley, D. R., Mullins, D. R., Ailey, K. S., and Radulovic, P. V., *J. Vac. Sci. Technol.* **A15**, 1647 (1997).
9. Loof, P., Kasemo, B., Andersson, S., and Frestad, F., *J. Catal.* **130**, 181 (1991).
10. Shelef, M., *Catal. Rev. Sci. Eng.* **11**, 1 (1975).
11. Zhang, X., Walters, A. B., and Vannice, M. A., *J. Catal.* **155**, 290 (1995).
12. Hadjiivanov, K., Bushev, V., Kantcheva, M., and Klissurski, D., *Langmuir* **10**, 464 (1994).
13. Chafik, T., Efstathiou, A., and Verykios, X. E., *J. Phys. Chem. B* **101**(40), 7968 (1997).
14. Dines, T. J., Rochester, C. H., and Ward, A. M., *J. Chem. Soc. Faraday Trans.* **87**, 643 (1991).
15. Boccuzzi, F., Guglielminotti, E., and Spoto, G., *Surf. Sci.* **251/252**, 1069 (1991).
16. Kugler, E. L., Kadet, A. B., and Gryder, J. W., *J. Catal.* **41**, 72 (1976).
17. Schraml-Marth, M., Wokaun, A., and Baiker, A., *J. Catal.* **138**, 306 (1992).
18. Niwa, M., Minami, T., Kodama, H., Hattori, T., and Murakami, Y., *J. Catal.* **53**, 207 (1978).
19. Sjoerd Kijlstra, W., Brands, D. S., Poels, E. K., and Blieck, F., *J. Catal.* **171**, 208 (1997).
20. Li, G., Kaneko, K., and Ozeki, S., *Langmuir* **13**, 5894 (1997).
21. Niwa, M., Furukawa, Y., and Murakami, Y., *J. Coll. Interface Sci.* **86**, 260 (1982).
22. Martinez-Arias, A., Soria, J., Conesa, J. C., Seoane, X. L., Arocoya, A., and Cataluna, R., *J. Chem. Soc. Faraday Trans.* **9**, 1679 (1995).
23. Guglielminotti, E., and Boccuzzi, F., *J. Mol. Catal. A* **104**, 273 (1996).
24. Trovarelli, A., *Catal. Rev. Sci. Eng.* **38**, 439 (1996).
25. Henrich, V. E., and Cox, P. A., "Surface Science of Metal Oxides." Cambridge Univ. Press, Cambridge, UK, 1994.
26. Mullins, D. R., Radulovic, P. V., and Overbury, S. H., *Surf. Sci.* **429**, 186 (1999).
27. Paranthaman, M., Goyal, A., List, F. A., Specht, E. D., Lee, D. F., Martin, P. M., He, Q., Christen, D. K., Norton, D. P., Budai, J. D., and Kroeger, D. M., *Physica C* **275**, 266 (1997).
28. Zhu, S., Lowndes, D. H., Budai, J. D., and Norton, D. P., *Appl. Phys. Lett.* **65**, 2012 (1994).
29. Mullins, D. R., Overbury, S. H., and Huntley, D. R., *Surface Sci.* **409**, 307 (1998).
30. Trudeau, M. L., Tshöpe, A., and Ying, J. Y., *Surf. Inter. Anal.* **23**, 219 (1995).
31. Umbach, E., Kulkarni, S., Feulner, P., and Menzel, D., *Surf. Sci.* **88**, 65 (1979).
32. Feulner, P., Kulkarni, S., Umbach, E., and Menzel, D., *Surf. Sci.* **99**, 489 (1980).
33. Umbach, E., and Menzel, D., *Chem. Phys. Lett.* **84**, 491 (1981).
34. Geisler, H., Odörfer, G., Illing, G., Jaeger, R., Freund, H. J.-F., Watson, G., Plummer, E. W., Neuber, M., and Neumann, M., *Surf. Sci.* **234**, 237 (1990); Esch, F., Ladas, S., Kennou, S., Siokou, A., and Imbihl, R., *Surf. Sci.* **355**, L253 (1996).
35. Carlson, T. A., "Photoelectron and Auger Spectroscopy." Plenum, New York, 1975.
36. Sokolowski, E., Nordling, C., and Siegbahn, K., *Phys. Rev.* **110**, 776 (1958).
37. Colton, R. J., and Rabalais, J. W., *Inorg. Chem.* **15**, 237 (1976).
38. Folkesson, B., *Acta Chem. Scand.* **27**, 287 (1973).
39. Fuggle, J. C., and Menzel, D., *Surf. Sci.* **79**, 1 (1979).
40. Kaneko, K., and Matsumoto, A., *J. Phys. Chem.* **93**, 8090 (1989).
41. Schwartz, J. M., and Schmidt, L. D., *J. Catal.* **148**, 22 (1994).
42. Padeste, C., Cant, N. W., and Trimm, D. L., *Catal. Lett.* **28**, 301 (1994).
43. Baldwin, E. K., and Friend, C. M., *J. Vac. Sci. Technol.* **A4**, 1407 (1986).
44. Pashutski, A., and Folman, M., *Surf. Sci.* **216**, 395 (1989).
45. Shirley, D. A., *Phys. Rev.* **B5**, 4709 (1972).
46. Kim, Y., Schreifels, J. A., and White, J. M., *Surf. Sci.* **114**, 349 (1982).